Structures and Phase Transition of Vaterite-Type Rare Earth Orthoborates: A Neutron Diffraction Study

Jianhua Lin,[†] Denis Sheptyakov,*[,‡] Yingxia Wang,[†] and Peter Allenspach[‡]

State Key Laboratory of Rare Earth Materials Chemistry and Applications, College of Chemistry and Molecular Engineering, Peking University, Beijing 100871, People's Republic of China, and Laboratory for Neutron Scattering, ETH Zürich & PSI Villigen, CH-5232 Villigen PSI, Switzerland

Received January 9, 2004. Revised Manuscript Received March 5, 2004

The structure of vaterite-type rare earth orthoborate ($LnBO_3$) has long been a subject of interest and controversy. In the present work, the crystal structures of two polymorphs of the vaterite-type rare earth orthoborates, i.e., the low- and high-temperature modifications of $(Y_{0.92}Er_{0.08})BO_3$, were solved and refined from neutron powder diffraction data. The low-temperature polymorph crystallizes in a C-centered monoclinic cell with *C*2/*c* space symmetry, the unit cell parameters being $a = 11.3138(3)$ Å, $b = 6.5403(2)$ Å, $c = 9.5499(2)$ Å, and $\beta = 112.902(1)°$. The boron atoms in the structure are all tetrahedrally coordinated and form the three-membered ring borate B_3O_9 groups. The high-temperature form crystallizes in a new structure type in a monoclinic cell with *C*2/*c* space symmetry, and the unit cell constants $a = 12.2019(3)$ Å, $b = 7.0671(2)$ Å, $c = 9.3424(2)$ Å, and $\beta = 115.347(1)°$. The borate groups in the high-temperature structure are all isolated flat BO_3 triangles. As far as the structural chemistry is concerned, both structures are different from the typical $CaCO_3$ vaterite. However, they do share some common features, particularly the packing fashion of the cations, which results in similarly looking X-ray diffraction patterns as that of the typical vaterite.

Introduction

Rare earth borates have been the subject of interest over the last several decades.[1−3] Recently, particular attention has been paid to these materials, motivated largely by their extraordinary optical properties.[4−12] Rare earth borates normally have high ultraviolet transparency and exceptional optical damage threshold, which makes them attractive for numerous practical applications, particularly in gas discharge panels. In the Ln_2O_3−B_2O_3 systems, three binary phases, i.e., oxyborate Ln_3BO_6, orthoborate $LnBO_3$, and metaborate $Ln(BO_2)_3$, were identified with high-temperature syntheses.[1−3] Additionally, some boron-rich phases have been reported recently: LnB_5O_9 was obtained by a low-temperature synthesis approach,[13−15] and the $Dy_4B_6O_{15}$[16] and $(Re)_2B_4O_9$ (Re = Eu, Gd, Tb, Dy)[17−19] oxoborates with the edge-sharing BO_4 tetrahedra were synthesized at high pressures and temperatures. Although most of the anhydrous rare earth borate phases were known for quite a long time, many controversies about the structures and even the composition remained to be clarified. For example, recently Corbel et al.[20] revised the crystal structure of L-$EuBO_3$ and assigned it to the space group $P\bar{1}$, similarly to the findings of Palkina et al.[21] for the case of L-$SmBO_3$. In addition, Lin et al.[22−24] had studied

* Corresponding author. E-mail: Denis.Cheptiakov@psi.ch.
† Peking University.
‡ ETH Zürich & PSI Villigen.

(1) Levin, E. M.; Robbins C. R.; Warring, J. L. *J. Am. Ceram. Soc.* **1961**, *44*, 87−91.
(2) Levin, E. M.; Roth, R. S.; Martin, J. B. *Am. Miner.* **1961**, *46*, 1030−1055.
(3) Leskelä, M.; Ninistö, L. *Handbook on the Physics and Chemistry of Rare Earths*; Gschneidner, K. A., Jr., Eyring, L., Ed.; Elsever Science Publishers: New York, 1986; Vol. 8, p 203.
(4) Hölsä, J. *Inorg. Chim. Acta* **1987**, *139*, 257−259.
(5) Chadeyron, G.; Mahiou, R.; EL-Ghozzi, M.; Arbus, A.; Zambon, D.; Cousseins, J. C. *J. Lumin.* **1997**, *72−74*, 564−566.
(6) Boyer, D.; Bertrand, G.; Mahiou,R. *J. Lumin.* **2003**, *104*, 229−237.
(7) Boyer, D.; Bertrand-Chadeyron, G.; Mahiou, R.; Caperaa, C.; Cousseins, J.-C. *J. Mater. Chem.* **1999**, *9*, 211−214.
(8) Bertrand-Chadeyron, G.; El-Ghozzi, M.; Boyer, D.; Mahiou, R.; Cousseins, J. C. *J. Alloys Compds.* **2001**, *317−318*, 183−185.
(9) Lemanceau, S.; Bertrand-Chadeyron, G.; Mahiou, R.; El-Ghozzi, M.; Cousseins, J. C.; Conflant, P.; Vannier, R. N. *J. Solid State Chem.* **1999**, *148*, 229−235.
(10) Lou, L.; Boyer, D.; Bertrand-Chadeyron, G.; Bernstein, E.; Mahiou, R.; Mugnier, J. *Opt. Mater.* **2000**, *15*, 1−6.
(11) Wei, Z. G.; Sun, L. D.; Liao, C. S.; Yin, J. L.; Jiang, X. C.; Yan, C. H. *J. Phys. Chem.* **2002**, *B 106*, 10610−10617.
(12) Wei, Z. G.; Sun, L. D.; Jiang, X. C.; Liao, C. S.; Yan, C. H.; Tao, Y.; Zhang, J.; Hu, T. D.; Xie, Y. N. *Chem. Mater.* **2003**, *15*, 3011−3017.
(13) Li, L. Y.; Lu, P. C.; Wang, Y. Y.; Jin, X. L.; Li, G. B.; Wang, Y. X.; You, L. P.; Lin, J. H. *Chem. Mater.* **2002**, *14*, 4963−4968.
(14) Li, L. Y.; Jin, X. L.; Li, G. B.; Wang, Y. X.; Liao, F. H.; Yao, G. Q.; Lin, J. H. *Chem. Mater.* **2003**, *15*, 2253.
(15) Lu, P. C.; Wang, Y. X.; Lin, J. H.; You, L. P. *Chem. Commun.* **2001**, 1178.
(16) Huppertz, H.; von der Eltz, B. *J. Am. Chem. Soc.* **2002**, *124*, 9376.
(17) Emme, H.; Huppertz, H. *Chem. Eur. J.* **2003**, *9*, 3623.
(18) Emme, H.; Huppertz, H. *Z. Anorg. Allg. Chem.* **2002**, *628*, 2165.
(19) Huppertz, H.; Altmannshofer, S.; Heymann, G. *J. Solid State Chem.* **2003**, *170*, 320.
(20) Corbel, G.; Leblanc, M.; Antic-Fidancev, E.; Lemaître-Blaise, M.; Krupa, J. C. *J. Alloys Compds.* **1999**, *287*, 71−78.
(21) Palkina, K. K.; Kuznetsov, V. G.; Butman, L. A.; Dzhurinskii, B. F. *Russ. J. Coord. Chem.* **1976**, *2*, 286−289.
(22) Lin, J. H.; Su, M. Z.; Wurst, K.; Schweda, E. *J. Solid State Chem.* **1996**, *126*, 287−291.
(23) Lin, J. H.; Zhou, S.; Yang, L. Q.; Yao, G. Q.; Su, M. Z. *J. Solid State Chem.* **1997**, *134*, 158−163.

10.1021/cm0499388 CCC: $27.50
Published on Web 05/15/2004

the crystal structures of La_3BO_6 and Y_3BO_6 and found that the compositions of these compounds should be $La_{26}(BO_3)_8O_{27}$ and $Y_{17.33}(BO_3)_4(B_2O_5)O_{16}$, respectively, instead of $LnBO_6$. However, the later NMR study of Y_3BO_6 indicated the presence of a BO_4 borate group in the structure.[25] The difficulty of precisely determining the crystal structure of rare earth borates originates mainly from the weak scattering power of boron and oxygen atoms for X-rays.

Similar difficulty was encountered for rare earth orthoborates. Depending on the cation size, the rare earth orthoborates crystallize with the aragonite,[26] H- or L-$SmBO_3$,[20,21] vaterite,[27,28] or calcite[29] type structure. Recently, Huppertz et al.[30] identified a new rare earth orthoborate, χ-$DyBO_3$, under high pressure and temperature (8 GPa, 1327 °C). Among these orthoborate phases, the structure of vaterite orthoborates was the most disputed. The vaterite structure was proposed for this rare earth orthoborate based on the similarity of its X-ray powder pattern to that of the $CaCO_3$ vaterite.[2] Newnham et al.[31] proposed two possible structure models: a distorted hexagonal structure in the space group $P6_3/mmc$, and an ordered one in $P6_3/mcm$. Bradley[32] described the structure with the space group $P\bar{6}c2$, in which the rare earth cations were proposed at the D_3 symmetry site. However, later spectroscopic studies using IR, NMR, and Raman techniques all indicated a tetrahedral coordination of boron atoms (B_3O_9) in the structure.[33−35] Recently, Chadeyron et al.[27] restudied the structure of YBO_3 using the single-crystal X-ray diffraction technique. They described the structure in a hexagonal cell, $a = 3.776$ Å and $c = 8.806$ Å, with the space group $P6_3/m$. Their structure model is similar to the disordered model by Newnham et al.,[31] which contains B_3O_9 units, but one oxygen and the boron sites are partially occupied (1/3). By using powder X-ray and electron diffraction techniques, one of us[28] found super-reflections corresponding to a rhombohedral cell, $a = 6.6357$ Å and $c = 20.706$ Å, for $GdBO_3$, but the proposed structure model was also questioned for its unphysical bond distances.

A parallel effort to characterize the vaterite-type rare earth orthoborate has been undertaken through the extensive spectroscopic investigations. In addition to previous IR, Raman, and ^{11}B MAS NMR experiments,[33−35] which confirmed the three-membered ring B_3O_9 borate unit, the recent spectroscopic study was focused mainly on the cation sites. However, the high-resolution luminescence spectra revealed a difficulty in unambiguously distinguishing between the alternatives of having either two[4,5] or three[6] cation sites in the structure. To clarify the structures of the vaterite-type rare earth orthoborates, one needs to use a technique that is more sensitive to light atoms. We report here the use of neutron diffraction as a complementary structure solution tool, since the coherent elastic scattering lengths of rare earths, oxygen, and boron for neutrons are of the same order of magnitude. The problem of the high absorption of neutrons by boron was overcome by using the ^{11}B isotope.

Experimental Section

Synthesis. The $(Y_{0.92}Er_{0.08})BO_3$ sample was prepared by solid-state reaction. The starting materials were Y_2O_3 (99.999%), Er_2O_3 (99.999%), and $H_3{}^{11}BO_3$ (Aldrich). A stoichiometric mixture of the starting materials (with 5 mol % excess of boric acid) was ground and preheated at 500 °C for 5 h. Then the powder was reground and heated at 1100 °C for 10 h. The product obtained was a white polycrystalline powder. Partial substitution of erbium for yttrium was done for a spectroscopic experiment besides the crystallographic study. Both $ErBO_3$ and YBO_3 are isostructural, thus there is no substantial influence on the crystallographic results.

Characterization. Powder X-ray diffraction patterns were recorded at room temperature on a Siemens D-500 diffractometer (Cu $K\alpha_{1,2}$ radiation) and with synchrotron radiation ($\lambda = 0.9531$ Å) at the powder diffraction station of the Materials Sciences Beamline of the Swiss Light Source (SLS). The difference scanning calorimetry (DSC) measurement was carried out with a "NETZSCN STA 449C" thermal analysis instrument. The neutron powder diffraction experiment was carried out with the HRPT neutron powder diffractometer at the Swiss Spallation Neutron Source (SINQ) in the temperature range between room temperature and 1000 °C. The neutron powder diffraction patterns (each containing 3200 points in the 2θ range from 3° to 163°) were recorded on heating. The sample was placed in a vanadium can of 5 mm diameter and 50 mm height. The neutron wavelengths used for the final refinements were 1.494 Å (room temperature) and 1.886 Å (high temperature). The structure determination and refinement of the high-T structure were performed on a dataset collected at 1000 °C.

Structure Determination of the Low-Temperature Polymorph. The X-ray and neutron powder diffraction patterns at room temperature could be indexed within a monoclinic cell, $a = 11.3138(3)$ Å, $b = 6.5403(2)$ Å, $c = 9.5499(2)$ Å, and $\beta = 112.902(1)°$, in the space group $C2/c$. This monoclinic lattice is related to the rhombohedral lattice observed in the electron diffraction[28] by removing the 3-fold axis. The main structural motive has then been solved from HRPT neutron powder data by using the direct methods implemented in the EXPO software kit[36] and refined using the program FULLPROF.[37] Thompson−Cox−Hastings pseudo-Voigt peak shape function was used, and the absorption correction was applied on the basis of the experimentally measured transmission of the incident neutron beam through the sample. Figure 1 shows the Rietveld refinement fit to the neutron powder diffraction pattern. The crystallographic data and selected bond distances are listed in the Tables 1 and 2.

Structure Determination of the High-Temperature Polymorph. The only available diffraction dataset—the neutron diffraction pattern collected with the HRPT diffractometer

(24) Lin, J. H.; You, L. P.; Lu, G. X.; Yang, L. Q.; Su, M. Z. *J. Mater. Chem.* **1998**, *8*, 1051−1054.
(25) Cohen-Adad, M. Th.; Aloui-Lebbou, O.; Goutaudier, C.; Panczer, G.; Dujardin, C.; Pedrini, C.; Florian, P.; Massiot, D.; Gerard, F.; Kappenstein, Ch. *J. Solid State Chem.* **2000**, *154*, 204−213.
(26) Antic-Fidancev, E.; Aride, J.; Chaminade, J.-P.; Lemaitre-Blaise, M.; Porcher, P. *J. Solid State Chem.* **1992**, *97*, 74−81.
(27) Chadeyron, G.; El-Ghozzi, M.; Mahiou, R.; Arbus A.; Cousseins, J. C. *J. Solid State Chem.* **1997**, *128*, 261−266.
(28) Ren, M.; Lin, J. H.; Dong, Y.; Yang, L. Q.; Su, M. Z.; You, L. P. *Chem. Mater.* **1999**, *11*, 1576−1580.
(29) Keszler, D. A.; Sun, H. *Acta Crystallogr. C* **1988**, *44*, 1505−1507.
(30) Huppertz, H.; von der Eltz, B.; Hoffmann, R.-D.; Piotrowski, H. *J. Solid State Chem.* **2002**, *166*, 203-212.
(31) Newnham, R. E.; Redman, M. J.; Santoro, R. P. *J. Am. Ceram. Soc.* **1963**, *46*, 253−256.
(32) Bradley, W. F.; Graf, D. L.; Roth, R. S. *Acta Crystallogr.* **1966**, *20*, 283−287.
(33) Laperches, J. P.; Tarte, P. *Spectrochim. Acta* **1966**, *22*, 1201−1210.
(34) Kriz, H. M.; Bray, P. J. *J. Chem. Phys.* **1969**, *51*, 3624−3625.
(35) Denning, J. H.; Ross, S. D. *Spectrochim. Acta* **1972**, *A28*, 1775−1785.
(36) Altomare, A.; Burla, M. C.; Camalli, M.; Carrozzini, B.; Cascarano, G. L.; Giacovazzo, C.; Guagliardi, A.; Moliterni, A. G. G.; Polidori, G.; Rizzi, R. *J. Appl. Crystallogr.* **1999**, *32*, 339−340.
(37) Roisnel, T.; Rodríguez-Carvajal, J. *Materials Science Forum* **2001**, *378−381*, 118−123.

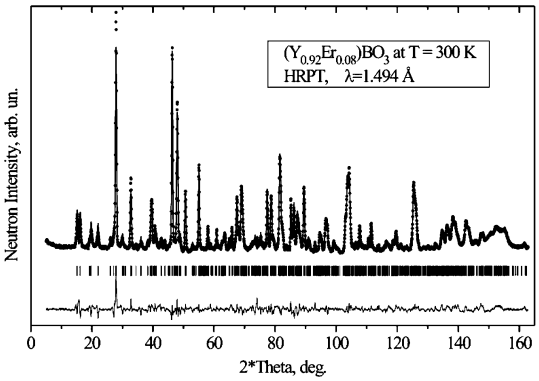

Figure 1. Rietveld fit of the $(Y_{0.92}Er_{0.08})BO_3$ crystal structure refinement from neutron powder diffraction data at room temperature. The observed data points, calculated profile, and difference curves are shown. The ticks correspond to the positions of Bragg peaks.

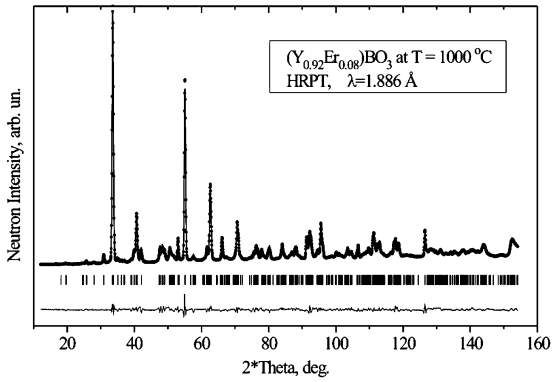

Figure 2. Rietveld fit of the $(Y_{0.92}Er_{0.08})BO_3$ crystal structure refinement from neutron powder diffraction data at 1000 °C. The observed data points, calculated profile, and difference curves are shown. The ticks correspond to the positions of Bragg peaks.

Table 1. Crystallographic Data of the Low-Temperature Phase of $(Y_{0.92}Er_{0.08})BO_3$

formula	$(Y_{0.92}Er_{0.08})BO_3$; $Z = 12$
space group	*C*2/*c*
lattice constants	$a = 11.3140(3)$ Å, $b = 6.5404(2)$ Å, $c = 9.5503(2)$ Å, $\beta = 112.902\ (1)°$
goodness of fit (χ^2)	12.7
Rp, Rwp	3.61%, 4.72%

atom	position	x	y	z
Y1/Er1	4c	0.25	0.25	0
Y2/Er2	8f	0.0843(5)	0.2561(6)	0.5007(8)
B1	8f	0.1220(5)	0.0382(9)	0.2476(5)
B2	4e	0	0.678(1)	0.25
O1	8f	0.1258(6)	0.083(1)	0.1057(5)
O2	8f	0.2209(5)	0.090(1)	0.3894(4)
O3	8f	0.0478(5)	0.565(1)	0.3938(5)
O4	8f	0.3932(6)	0.309(1)	0.2543(7)
O5	4e	0	0.1399(17)	0.25

Table 2. Selected Bond Distances and Angles in the Structure of the Low-Temperature Phase of $(Y_{0.92}Er_{0.08})BO_3$

bond	value (Å)	bond/angle	value (Å/deg)
Y1−O1 ×2	2.301(7)	B1−O2	1.423(7)
Y1−O2 ×2	2.431(6)	B1−O4	1.506(8)
Y1−O3 ×2	2.435(6)	B1−O5	1.540(8)
Y1−O4 ×2	2.369(6)	B2−O3 ×2	1.467(6)
Y2−O1	2.467(9)	B2−O4 ×2	1.495(8)
Y2−O1	2.403(10)	O1−B1−O4	104.0(7)
Y2−O2	2.444(8)	O1−B1−O5	106.8(6)
Y2−O2	2.274(8)	O2−B1−O4	107.1(7)
Y2−O3	2.226(8)	O2−B1−O5	105.0(5)
Y2−O3	2.407(9)	O4−B1−O5	109.3(8)
Y2−O4	2.293(9)	O3−B2−O4 ×2	105.8(7)
Y2−O5	2.333(8)	O3−B2−O4 ×2	108.0(7)
B1−O1	1.403(7)	O4−B2−O4	110.0(8)

at 1000 °C—was indexed in the monoclinic unit cell with *C*2/*c* symmetry and the parameters $a = 12.2019(3)$ Å, $b = 7.0671(2)$ Å, $c = 9.3424(2)$ Å, and $\beta = 115.347\ (1)°$. The initial basic structural motive was then derived from the HRPT neutron powder diffraction pattern with the use of the program suite FOX.[38] However, only the detailed iterative procedure including the analysis of Fourier maps and Rietveld refinements allowed us to find the exact solution, suitable for the final refinement. Figure 2 shows the Rietveld refinement fit of the neutron diffraction pattern. The crystallographic data and selected bond distances are listed in the Tables 3 and 4.

(38) Favre-Nicolin, V.; Cerný, R. *J. Appl. Crystallogr.* **2002**, *35*, 734−743.

Table 3. Crystallographic Data of the High-Temperature Phase of $(Y_{0.92}Er_{0.08})BO_3$ at $T = 1000$ °C

formula	$(Y_{0.92}Er_{0.08})BO_3$; $Z = 12$
space group	*C*2/*c*
lattice constants	$a = 12.2019(3)$ Å, $b = 7.0671(2)$ Å, $c = 9.3424(2)$ Å, $\beta = 115.347\ (1)°$
goodness of fit	16.8
Rp, Rwp	3.77%, 5.01%

atom	position	x	y	z
Y1/Er1	4c	0.25	0.25	0
Y2/Er2	8f	0.0764 (4)	0.2578 (6)	0.4989 (6)
B1	8f	0.1818 (7)	0.4023 (9)	0.2631 (6)
B2	4e	0	0.9271 (18)	0.25
O1	8f	0.0934 (6)	0.4480 (13)	0.1200 (7)
O2	8f	0.2012 (7)	0.4361 (9)	0.4086 (6)
O3	8f	0.0480 (7)	0.8872 (14)	0.3943 (7)
O4	8f	0.2820 (7)	0.3045 (11)	0.2540 (6)
O5	4e	0	0.1596 (12)	0.25

Table 4. Selected Bond Distances and Angles in the Crystal Structure of the High-Temperature Phase of $(Y_{0.92}Er_{0.08})BO_3$ at $T = 1000$ °C

bond	value (Å)	bond/angle	value (Å/deg)
Y1−O1 ×2	2.950(8)	Y2−O5	2.214(6)
Y1−O2 ×2	2.360(7)	B1−O1	1.350(9)
Y1−O3 ×2	2.431(9)	B1−O2	1.298(8)
Y1−O4 ×2	2.267(6)	B1−O4	1.439(12)
Y2−O1	2.315(10)	B2−O3 ×2	1.251(7)
Y2−O1	2.334(10)	B2−O5	1.643(15)
Y2−O2	2.392(10)	O1−B1−O4	113.3(9)
Y2−O2	2.826(10)	O2−B1−O4	111.9(9)
Y2−O3	2.765(11)	O1−B1−O2	134.8(8)
Y2−O3	2.375(10)	O3−B2−O5 ×2	103.1(9)
Y2−O4	2.257(8)	O3−B2−O3	153.9(8)

Results and Discussion

Structure of the Low-Temperature Polymorph. Figure 3a shows a projection of the crystal structure of the low-temperature phase of $(Y_{0.92}Er_{0.08})BO_3$ vaterite along the *b*-axis. The structure could be described as alternative stacking of cation sheets and borate layers. The boron atoms are all tetrahedrally coordinated in the BO_4 units, which share vertices, thus forming three-membered ring borate B_3O_9 units. The B−O bond distances are all typical for tetrahedral borate groups, ranging from 1.403 to 1.540 Å. Figure 3b presents another view of the structure projected along the (001) direction. It can be seen that the yttrium atoms adopt the layers of the almost ideal close-packed arrangement. The two yttrium atoms, Y1 (4c) and Y2 (8f), are all

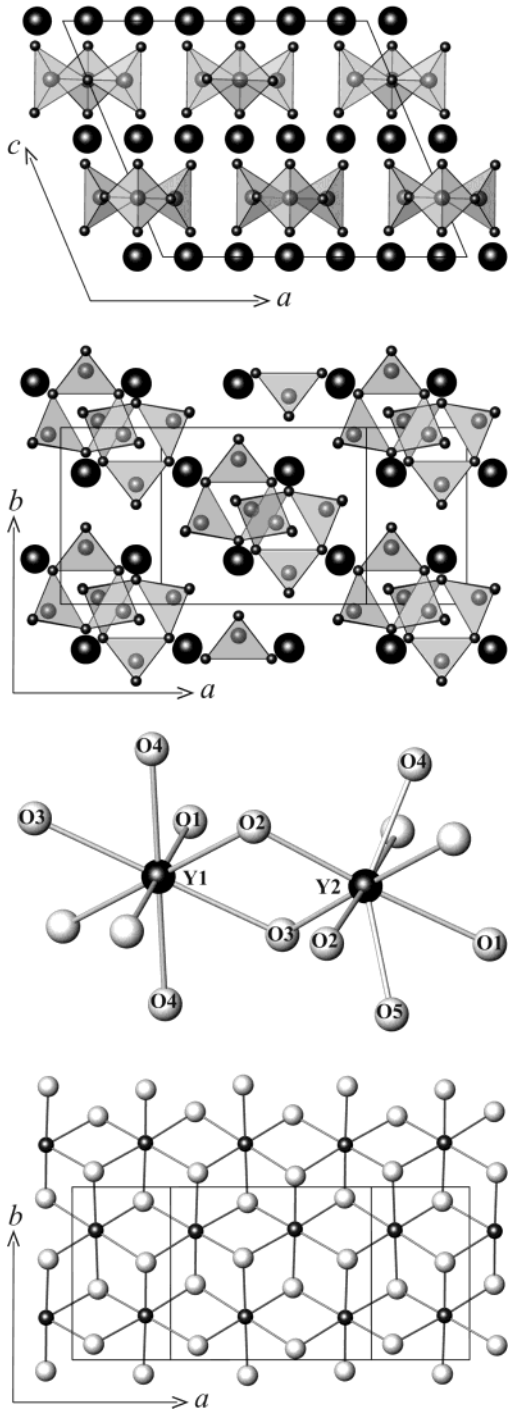

Figure 3. (a) Projection of the structure of the low-temperature phase $(Y_{0.92}Er_{0.08})BO_3$ along the *b*-axis. (b) Projection of the structure of the low-temperature phase $(Y_{0.92}Er_{0.08})BO_3$ along the (001) direction. (c) Coordination polyhedra of Y1 and Y2 atoms. (d) The structure of the $[YO_2]$ layer in the low-temperature polymorph of $(Y_{0.92}Er_{0.08})BO_3$. The packing fashion of ions is similar to that in the (111) rock salt layer: dark, smaller balls represent the Y cations, and the oxygens are plotted as bigger, light balls.

8-coordinated, as shown in Figure 3c. The coordinating oxygens could be sorted into two groups: the terminal oxygens in the B_3O_9 units (i.e., O1, O2, and O3) coordinate the yttrium atoms as a trigonal antiprism, thus forming a (111) rock salt layer $[YO_2]$ as shown in Figure 3d; the bridged oxygens (i.e., O4 and O5) further coordinate the cations, resulting in two coordination polyhedra with point symmetry of C_i for Y1 and C_1 for Y2, respectively.

It is noteworthy that the carbon atoms in the typical $CaCO_3$ vaterite[39] are triangularly coordinated, so its structure is different from the low-temperature YBO_3 orthoborate. However, both structures contain the rock salt layers that stack in exactly the same sequence as AbC|CbA|AbC, where the capital letters represent the oxygens and small letters the cations. The only difference of these two structures is the position of boron/carbon and the bridged oxygen. The contribution of scattering from these atoms to the X-ray diffraction pattern is relatively weak, so that both compounds may show similar X-ray patterns,[1] although the exact ordering of anions in the structures is different.

As indicated above, the monoclinic cell can be derived from the pseudorhombohedral lattice observed in electron diffraction[28] by removing the 3-fold axis, which further demonstrates the completeness of the monoclinic setting. The hexagonal cell ($a = 3.776$ Å and $c = 8.806$ Å) in Chadeyron's structure model[27] is only a subcell setting of the pseudorhombohedral cell, which may be derived by neglecting the weak super-reflections. The hexagonal model could provide a quite accurate description for the $[YO_2]$ part of the YBO_3 structure, since the ideal rock salt layer packing is preserved in this subcell. The boron and bridged oxygen atoms, however, cannot be completely defined in this subcell, which has to be expressed by random distribution within the 6h sites in the hexagonal model. In every sense the hexagonal structure is an averaged structure model, which could represent the major structural features of the vaterite orthoborates but not the structural details.

It is interesting to correlate the crystal structure with the known spectroscopic results of the Eu^{3+}-doped YBO_3, since this compound is in fact an important luminescent material used in plasma display panels or mercury-free lamps. The luminescence spectrum of the Eu^{3+} ion is very sensitive to the local symmetry of the doped cation sites and has been widely used as a structural probe. Using high-resolution luminescence spectrum, Hölsä[4] identified two cation sites in YBO_3:Eu and assigned them to the point symmetries D_{3d} and T. Recently, Chadeyron et al.[5] identified three $^5D_0-^7F_0$ peaks and attributed two of them to the intrinsic cation sites (C_3 symmetry) and another one, the intensity of which depends strongly on the synthesis conditions, to a perturbed cation site. Alternatively, Boyer et al.[6] proposed three intrinsic cation sites based on the hexagonal model. They inferred the three possible local environments for the cations by distributing the bridged oxygens in an ordered way. The derived polyhedra have the same geometry as those observed in our monoclinic structure model, except for the fact that the Y2 (8f) site was described with two polyhedra with a slight difference in bond distances and angles. From the structural point of view, this description implies lower symmetry and an enlarged unit cell. Having the pseudorhombohedral lattice preserved, the symmetry could be further reduced to the triclinic $P\bar{1}$ by removing the 2-fold axis from the monoclinic cell. The cell volume of this hypothetical triclinic structure should be 3 times that of the

(39) Meyer, H.-J. *Fortsch. Mineral.* **1960**, *38*, 186.

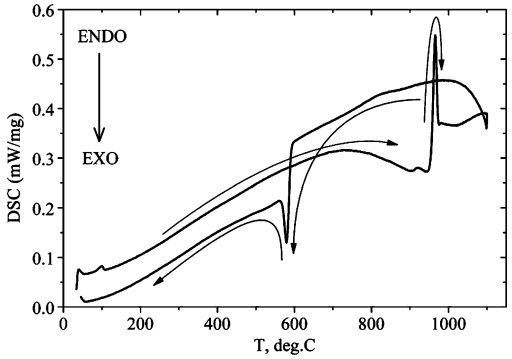

Figure 4. DSC signal curve of $(Y_{0.92}Er_{0.08})BO_3$, which shows large thermal hysteresis upon heating and cooling. The thin arrows are indicating the temperature history.

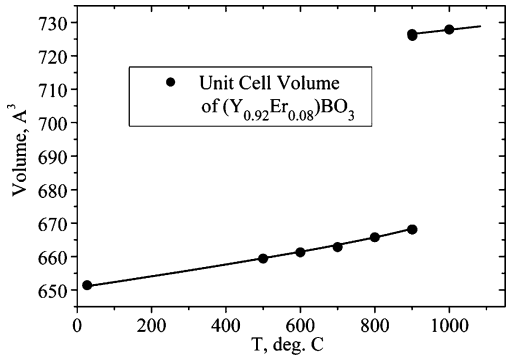

Figure 5. Temperature dependence of the unit cell volume of $(Y_{0.92}Er_{0.08})BO_3$, as refined from the neutron powder data taken on heating.

hexagonal cell, in which four cation positions could be readily derived: two at the inversion centers and two at general positions. On the other hand, the ^{89}Y MAS NMR study unambiguously showed two distinct Y sites with a ratio of about 1:2 in YBO_3,[25] which agrees perfectly with the cation distribution (Y1 (4c) and Y2 (8f)) in our monoclinic structure model.

Of course, certain caution should be taken in using the luminescence probe to interpret the structural properties. The luminescence spectra of Eu^{3+} do provide symmetry information around the probe centers. However, they are also very sensitive to the distortions induced by the probe itself or by imperfections in the crystals. A recent XAFS study[11] on YBO_3:Eu showed that the nanosized particles do suffer considerable lattice disorder that consequently has significant influence on the luminescence spectra.[12] Anyhow, the experimental evidences available at the present stage are not sufficient to support a further symmetry reduction of the monoclinic structure, whereas as far as all evidence is concerned, the monoclinic structure is the most appropriate model for the vaterite-type rare earth orthoborates.

Phase Transformation and the Structure of the High-Temperature Polymorph. The phase transition and the presence of the unquenchable high-temperature polymorph were observed many years ago by Levin et al.[1] for the vaterite rare earth orthoborates. To investigate the structure of the high-temperature phase, we restudied the phase transformation process. Figure 4 shows the DSC curves of $(Y_{0.92}Er_{0.08})BO_3$ on heating and cooling. $(Y_{0.92}Er_{0.08})BO_3$ transforms to the high-temperature polymorph at about 965 °C on heating and returns

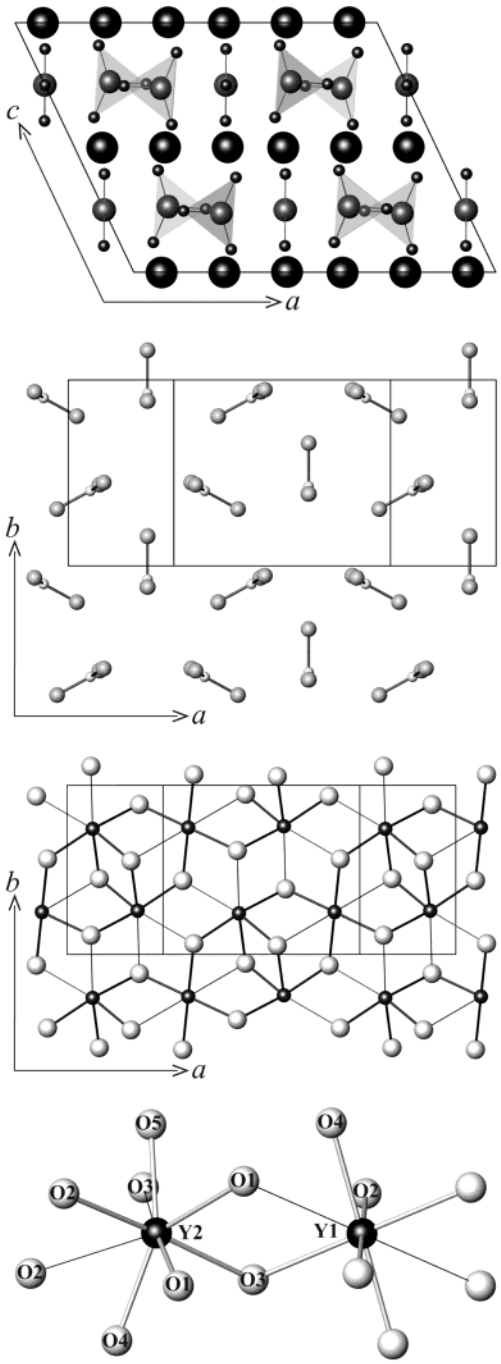

Figure 6. (a) Projection of the structure of the high-temperature $(Y_{0.92}Er_{0.08})BO_3$ phase along the *b*-axis. (b) Orientation arrangement of BO_3 groups in the structure of high-temperature polymorph. The view of the crystal structure along the (001) direction. (c) The $[YO_2]$ layer in the high-temperature crystal structure of $(Y_{0.92}Er_{0.08})BO_3$. (d) Coordination polyhedra of Y1 and Y2 in the structure of the high-temperature phase of $(Y_{0.92}Er_{0.08})BO_3$. The thick lines in drawings c and d represent the actual bonds, while the thin lines represent longer distances ranging from 2.76 to 2.95 Å.

to the low-temperature form at about 580 °C during cooling. The observed large hysteresis is consistent with the results for the other vaterite orthoborates.[1,28] The structure of the high-temperature phase was initially solved from the HRPT neutron powder data using a nonstandard setting of the $C2/c$ space group (namely, $I2/c$) with the lattice parameters: $a' = 11.7692(3)$ Å, $b' = 7.0674(2)$ Å, $c' = 9.3436(3)$ Å, and $\beta' = 110.477(2)°$.

Table 5. Summary of the Lattice Parameters of Selected Rare Earth Orthoborates and $CaCO_3$[a]

structure type	compd	a (Å)	b (Å)	c (Å)	β (deg)	space group	a_r (Å)	c_r (Å)	a_r/c_r
aragonite	$CaCO_3$	4.961	7.967	5.741		*Pmcn*	4.693	2.870	1.635
aragonite	$LaBO_3$	5.104	8.252	5.872		*Pmcn*	4.851	2.936	1.652
vaterite	$CaCO_3$	4.13	7.15	8.48		*Pbnm*	4.130	4.240	0.974
vaterite	YBO_3−H	12.205	7.067	9.344	115.4	*C*2/*c*	4.067	4.224	0.963
vaterite	YBO_3−L	11.314	6.540	9.550	112.9	*C*2/*c*	3.771	4.399	0.857
vaterite	$LuBO_3$−H	3.727		8.722		*P*63/*mmc*	3.727	4.361	0.855
calcite	$CaCO_3$	4.989		17.053		$R\bar{3}c$	4.989	2.842	1.755
calcite	$LuBO_3$	4.915		16.212		$R\bar{3}c$	4.915	2.702	1.819

[a] The meaning of the last three columns, the reduced lattice parameters, is explained in the text.

To provide an easier comparison to the low-temperature form, the final refinements have been carried out in the standard setting of the same group *C*2/*c*, with the unit cell parameters, $a = 12.2019$ Å, $b = 7.0671$ Å, $c = 9.3424$ Å, and $\beta = 115.347°$. It can be seen that upon the phase transition, the structure expands in the $a-b$ (YO_2) plane and contracts along the (001) direction. Figure 5 shows the variation of the unit cell volume of $(Y_{0.92}Er_{0.08})BO_3$ with temperature as refined from the neutron diffraction data. Both phases exhibit a similar thermal expansion, but a discontinuous volume change occurs at the phase transition point.

It is instructive to compare the lattice parameters of the rare earth orthoborates and $CaCO_3$. In Table 5, we summarize the lattice constants for rare earth orthoborates and calcium carbonates. Regardless of what is the exact symmetry of the compounds listed in Table 5, the pseudoprimary cell of these orthoborates and carbonates can always be roughly described by the hexagonal cell setting. The parameters a_r and c_r of the reduced cell (which we define as a pseudohexagonal primary cell containing only one $LnBO_3$ formula unit) are also included in Table 5. The ratios of these reduced cell parameters a_r and c_r are further used to classify the structure types. The calcite and aragonite structures normally have a large reduced a_r/c_r ratio, since the triangular anions have a nearly parallel arrangement within the $a-b$ plane. The difference between the calcite and the aragonite structures is the position of the triangular anions controlled mainly by the cation radii and the required coordination number, i.e., 6-coordinated in calcite and 9-coordinated in aragonite, respectively. On the other hand, the triangular anions are vertically arranged in the vaterite structure, leading to a smaller a_r/c_r ratio. In addition, the vaterite structures may be further classified into two groups. The low-temperature orthoborate structure exhibits an even smaller a_r/c_r than the high-temperature orthoborate and the vaterite $CaCO_3$. Considering that the boron atoms are also triangularly coordinated in the high-temperature orthoborate, as revealed by high-temperature ^{11}B NMR measurements,[25] the structure of the high-temperature orthoborate is closer to that of the typical vaterite.

Figure 6a shows a projection of the structure of the high-temperature $(Y_{0.92}Er_{0.08})BO_3$ along the *b*-axis. This new structure type can also be described as alternative stacking of triangular BO_3 borate layers and rare earth cation layers as that in the typical $CaCO_3$ vaterite. However, the orientation of the triangular borate groups is different, as shown in Figure 6b. In the typical vaterite $CaCO_3$, the triangular anion groups are parallel, whereas in the high-temperature form of YBO_3 they are related by a pseudo-3-fold axis. The arrangement of the BO_3 can be traced back to the structure of the B_3O_9 groups in the low-temperature phase. In the high-temperature phase, three B−O bonds in the cyclic B_3O_9 groups are broken, whereas the cation arrays maintain their close-packed layer. The surrounding of boron atoms in the high-temperature phase of $(Y_{0.92}Er_{0.08})BO_3$ is less symmetric than that in the low-temperature modification. This may easily be seen from comparison of the values of B−O interatomic distances and O−B−O bond angles in them (Tables 2 and 4). The coordination triangle around the B2 atom is even more distorted than that around the B1 atom. Interestingly, the high-pressure structure (χ-$DyBO_3$) established by Huppertz et al.[30] can be considered as an intermediate phase between the low- and high-temperature polymorphs presented in this study, in which only one B−O bond in the cyclic B_3O_9 groups is broken, leading to an open B_3O_9 group consisting of two BO_4 and one BO_3. Figure 6c shows the structure of the [YO_2] layer. One can see that the oxygen atoms are shifted so that the Y atoms are coordinated only by four oxygen atoms within the [YO_2], as indicated by the thick lines in the figure. The terminal oxygen atoms connected by the thin lines stay away from Y atoms in the range from 2.76 to 2.95 Å, which should not be included in the coordination polyhedra. The O4 and O5 also coordinate the rare earth cations; thus the rare earth cations are all 6-coordinated in the high-temperature structure (Figure 6d).

In conclusion, the crystal structures of the low- and high-temperature polymorphs of vaterite rare earth orthoborate were established from neutron powder diffraction. In the low-temperature structure, boron atoms are all tetrahedrally coordinated and form B_3O_9 units. In the high-temperature polymorph, the boron atoms are all in triangular coordination. As far as the structure is concerned, both phases are not the typical vaterite structure. However, they do retain some structural features typical for vaterite. In the high-temperature form, the triangular borates are all vertically arranged with respect to the cation layers. The low-temperature form, on the other hand, could be considered as a derivative of the high-temperature form via addition of B−O bonds. The cations in both structures adopt the close-packed arrays similar to that in the $CaCO_3$ vaterite. These structural features give rise to a similar powder diffraction pattern as that of the $CaCO_3$ vaterite, particularly for X-ray diffraction, which was the reason for assigning them to the vaterite structure type in earlier studies. Moreover, the monoclinic structure of the low-temperature phase can be well used to interpret the results of the spectroscopic studies.

Acknowledgment. J.L. thanks the financial support from NSFC (20221101 and 20371005) and State Key Basic Research Program of China. This work was partly performed at the spallation neutron source SINQ and the synchrotron radiation source SLS at the Paul Scherrer Institute, Villigen, Switzerland. We thank Dr. K. Conder for the DSC measurements.

CM0499388